Reconstruction of three-dimensional porous media from a single two-dimensional image using three-step sampling

MingLiang Gao,[1,2] XiaoHai He,[1,*] QiZhi Teng,[1] Chen Zuo,[1] and DongDong Chen[1]
[1]*College of Electronics and Information Engineering, Sichuan University, Chengdu 610065, China*
[2]*Northwest University for Nationalities, College of Electrical Engineering, Lanzhou 730030, China*
(Received 9 November 2014; published 26 January 2015)

A random three-dimensional (3D) porous medium can be reconstructed from a two-dimensional (2D) image by reconstructing an image from the original 2D image, and then repeatedly using the result to reconstruct the next 2D image. The reconstructed images are then stacked together to generate the entire reconstructed 3D porous medium. To perform this successfully, a very important issue must be addressed, i.e., controlling the continuity and variability among adjacent layers. Continuity and variability, which are consistent with the statistics characteristic of the training image (TI), ensure that the reconstructed result matches the TI. By selecting the number and location of the sampling points in the sampling process, the continuity and variability can be controlled directly, and thus the characteristics of the reconstructed image can be controlled indirectly. In this paper, we propose and develop an original sampling method called three-step sampling. In our sampling method, sampling points are extracted successively from the center of 5×5 and 3×3 sampling templates and the edge area based on a two-point correlation function. The continuity and variability of adjacent layers were considered during the three steps of the sampling process. Our method was tested on a Berea sandstone sample, and the reconstructed result was compared with the original sample, using tests involving porosity distribution, the lineal path function, the autocorrelation function, the pore and throat size distributions, and two-phase flow relative permeabilities. The comparison indicates that many statistical characteristics of the reconstructed result match with the TI and the reference 3D medium perfectly.

DOI: 10.1103/PhysRevE.91.013308 PACS number(s): 02.70.−c, 81.05.Rm, 47.56.+r

I. INTRODUCTION

A variety of methods have been used to reconstruct a three-dimensional (3D) porous medium from a two-dimensional (2D) image, but in its early days, such reconstruction was dominated by two main approaches, two-point statistics modeling and object-based modeling [1–3]. Two-point statistics programs use a pixel-based simulation approach, whereby grid nodes are simulated one at a time. Even though all of the characteristics of a two-point statistics reconstruction might be perfect, they cannot capture curvilinear or other geometrically complex heterogeneity features, such as channels that typically have a first-order impact on reservoir connectivity and flow behavior [4,5], because they are limited to two-point statistics. Object-based programs allow reproduction of those important features, but they traditionally suffer from severe data conditioning limitations, especially when the size of the objects is larger than the average spacing between hard data, or when exhaustive soft data sets need to be integrated.

These shortcomings have led to the development of a method based on multiple-point statistics (MPS), an accurate algorithm for addressing some of the problems. MPS simulation aims at combining the data conditioning flexibility of variogram-based programs with the ability of object-based programs to reproduce geologically realistic features. Therefore, one can expect the complex structure in a reservoir to be reproduced more accurately, because the MPS method considers more than two points at a time.

The main idea of MPS, introduced by Guardiano and Srivastava [6], extended normal equation simulation (ENESIM), consists in extracting multiple-point patterns from training images (TIs), and then reproducing those training patterns that match reservoir local data. However, the original MPS algorithm was impractical, because the method was required to rescan the TI to simulate each new data event and consequently was extremely demanding of central processing unit (CPU) usage. Strebelle [7–9] proposed an alternative method, single normal equation simulation (SNESIM), using a search tree structure, an efficient method of accessing high-dimensional data that can overcome the problems associated with the original MPS method. Subsequently, MPS was used in geostatistics modeling and other research.

However, memory and speed issues can arise in the case of geometrically complex multiphase TIs, and SNESIM can be computation time intensive, when applied to multimillion-cell grids. Three main research avenues have been investigated in recent years to overcome those issues.

The first research avenue consists in simulating blocks of pixels instead of an individual pixel. In SIMPAT, proposed by Arpat and Caers [10,11], training patterns are grouped into clusters based on a distance function, and each cluster is represented by a pattern prototype. Because of the limited number of clusters, storing pattern prototypes requires much less memory than does using a search tree. However, three-dimensional simulation using SIMPAT can be extremely slow, and dense conditioning data can be difficult to handle. Another pattern-based approach, FILTERSIM, proposed by Zhang *et al.* [12], introduces filters to summarize high-dimensional patterns into a small set of filter scores, which are then used to classify patterns into a limited number of classes. Although the filters help to speed up the simulation of patterns, significant discontinuities between simulated patterns are commonly observed in FILTERSIM realizations. In CCSIM, proposed recently by Tahmasebi and co-workers [13–15],

*Corresponding author: hxh@scu.edu.cn

a cross-correlation function and a grid splitting technique are used to determine the matching patch (pattern) in the reconstruction. Not only the speed, but also the accuracy noticeably improved.

The second research avenue consists in proposing alternatives to SNESIM'S search trees. Straubhaar *et al.* [16–18] replaced those trees with allocated lists in IMPALA, and Xu *et al.* [19] replaced them with another data structure, arrays, thereby enabling code parallelization and substantial improvements in reconstruction speed. Mariethoz *et al.* [20,21] modified the original ENESIM program by implementing a direct sampling (DS) approach, whereby the scanning of the training image is stopped as soon as a pattern similar to the conditioning data event is found; the central value of that pattern is directly inserted into the simulation grid. The DS approach is much faster than the repetitive scanning of the entire training image in ENESIM.

The third research avenue, proposed by Tran [22], consists in applying a multiple grid and effectively solved the conflict of precision with speed and memory as a result of using a single large template. Based on original multiple grid, Strebelle and Claude [7] proposed a new kind of multiple grid, improving speed and reducing memory usage further, while ensuring the accuracy of the reconstruction, thereby injecting the SNESIM with new vitality.

Reconstructing 3D structure can involve using one 2D TI or multiple 2D TIs. All of the information depicting the subsurface heterogeneity and geological features that mainly represent the spatial continuity, patterns, and distribution of the available features in a reservoir are extracted only from the TI, so a reconstruction based on one TI must assume that the statistics of a reconstructed 3D volume is consistent with the 2D training image, or at least that the statistical information of the missing dimension can be represented by any direction's statistical information from the TI, with further cases assuming that the 3D volume is isotropic. An anisotropic 3D spatial object can be reconstructed based on multiple TIs, and different images can represent different directions' statistics of the 3D volume.

Two types of method have been investigated for reconstructing a 3D medium using one TI, directly by 3D volume and layer by layer. The model proposed by Okabe and Blunt [23,24] is of the former type. To generate a 3D structure from a 2D TI, measured multiple-point statistics on one plane are rotated 90° around each principal axis. In other words, measured statistics on the *XY* plane are transformed to the *XZ* and the *YZ* planes with an assumption of isotropy in orthogonal directions. At every voxel to be assigned a pore or grain phase, three principal orthogonal planes, *XY*, *XZ*, and *YZ*, intersecting this voxel are used to find conditioning data on these planes individually. Each probability of the phase at this voxel on the different planes is estimated by this process, and then the three measured probabilities are weighted by the number of conditioning data on each plane to obtain a single probability for this voxel. Finally, the phase at the voxel is assigned based on this weighted probability to generate a 3D image. The result has favorable connectivity, but the original data and weighted value are difficult to set.

The latter approach is based on regarding the 3D volume as stacked in a series of layers, with a next layer being able to be reconstructed conditionally with sampled data from the previous layer; the methods introduced by Tahmasebi *et al.* [13–15,25] and Hajizadeh *et al.* [26] belong to this approach. The advantage of this method is that with sampling data, the features of a layer can be carried neatly to the next layer. The sampling process is a key component of this approach.

Different kinds of sampling methods have been proposed, such as that of Tahmasebi *et al.* [13–15] using the CCSIM algorithm. This is achieved using *quadtrees*, a nonuniform or adaptive sampling method that partitions the image into subsections based on Shannon entropy and then selects a specified percentage of sampling data according to a set criterion. That method acts on continuity perfectly in practical application, but its variability is difficult to control.

Hajizadeh *et al.* [26] proposed another sampling method. The procedure is started by selecting a sampling template with a size of approximately 31×31 consistent with the largest pore in the image. The image is scanned with this sampling template; the central node of any sampling template that is entirely pore (grain) is marked as hard data, and the remaining pixels in the template are excluded as potential conditioning data. The sampling template size is then reduced by 2 to 29×29, and the image is scanned to select the conditioning data present at this scale. The procedure is repeated until the smallest 3×3 sampling template size is reached. Finally, appropriate data belonging to the center of those sampling templates with a specific size are selected as hard data based on the sampling rate. The smallest size of the sampling template is approximately 3×3; hence pores (grains) with size less than 3×3 cannot be sampled. However, the specific shape of pore or grain is confirmed by these details [27], so the reconstruction has poor continuity, especially when the scanning template for extracting patterns is small.

In this paper, a two-phase 3D porous medium is reconstructed from one 2D TI using a layer-by-layer MPS-based method, three-step sampling, as follows. (1) sampling the sample with template of size 5×5, (2) sampling the remainder of the sample with template of size 3×3, by the first two steps, the basic form of the pore (grain) is "carried" to the next layer, and (3) sampling the edge area of the sample using the two-point correlation function as a restrictive condition. The continuity and variability of adjacent layers were taken into full account and were ensured to match the statistics characteristics of TI at the sampling process. The two phases of a porous medium are called pore and grain, respectively, in this paper to simplify the discussion.

The remainder of the paper is organized as follows. The MPS algorithm is described In Sec. II. Section III presents the three-step sampling method. Section IV describes the results, including a demonstration of the efficiency of the proposed algorithm. The paper is summarized in Sec. V.

II. SNESIM ALGORITHM AND MULTIGRID APPROACH

A. A brief review of the SNESIM algorithm

SNESIM, the method proposed by Strebelle [7–9], combines easy conditioning of pixel-based algorithms with the ability to reproduce patterns of object-based algorithms. The complex

geological structures expected to be present at field scale are characterized by multiple-point statistics. Such multiple-point statistics can be read from TIs and then exported to the model, where they are anchored to the conditioning data using a pixel-based sequential simulation algorithm.

All patterns are derived from the TI, which has rigorous constraints [23,28]. The procedure for reconstructing a 3D volume includes two steps: extracted multiple-point statistics from the TI and pattern reproduction. A scanning template T_n is composed of n locations l_α and a central location l_c:

$$T_n = l_c + l_\alpha \quad \alpha = 1, \ldots, n. \tag{1}$$

The TI is scanned by the scanning template T_n to collect the pattern P_i at each location i. The pattern can be defined by

$$P_i = \{u_{ic} + u_{i\alpha}\, \alpha = 1, \ldots, n\}. \tag{2}$$

Each grid in the scanning template has a number to identify the pattern. The set storing all the patterns scanned from the TI is called the pattern set and is written as

$$\text{Set} = (P_i, i = 1, \ldots, N). \tag{3}$$

N is the number of different central locations of the scanning template over the TI. However, there are fewer than N patterns, because many patterns are the same.

The nature of reconstruction based on multiple-point statistics is to put the simulating grid on the scanning template center and determine the pixel value based on a portion of known condition data. The pixel value can be calculated by comparing the probabilities of occurrence of patterns composed by those portions of the condition data. The probability, the conditional probability distribution function (CPDF), can be expressed as follows:

$$P_r\left\{P_i|_{u_c=s_k}/P_i\right\} = \frac{P_r\{u_c = s_k \text{ and } u_\alpha = s_\alpha\}}{P_r\{u_\alpha = s_\alpha\}}, \quad \alpha, k = 1, \ldots, n. \tag{4}$$

The formula indicates the probability of the grid u_c to be calculated for the states $s_k, k = 1, \ldots, j$ based on the condition data $u_\alpha = s_\alpha, \alpha = 1, \ldots, n$. The formula can also be expressed as follows:

$$P_r\left\{P_i|_{u_c=s_k}\right\} = \frac{T(p_i|_{u_c=s_k})}{T(p_i)}. \tag{5}$$

$T(p_i|_{u_c=s_k})$ is the number of repetitions of pattern P_i with the grid $u_c = s_k$, and $T(p_i)$ is the number of repetitions of pattern P_i. Under the same condition data, the value of grid u_c can also be expressed as

$$s_k = s_q|_{\max[T(p_i|_{u_c=s_q})]}, \quad k, q = 1, \ldots, j. \tag{6}$$

B. The multigrid approach

Based on MPS, the reconstruction's accuracy, computer memory, and speed are directly related to the scanning template size. The larger the template size, the more patterns are obtained, especially the large-scale structures; hence, the reconstruction is very accurate, but computer memory usage increases sharply and speed decreases sharply. An alternative multigrid approach introduced by Strebelle [7–9] can resolve this conflict effectively. Computer memory and time can be reduced greatly, retaining accuracy, using that approach.

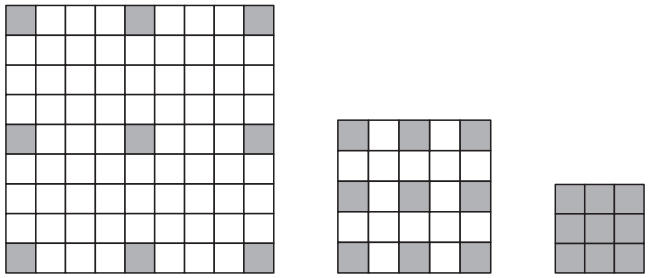

FIG. 1. Three-grid: (a) the coarsest grid; (b) the finer grid; (c) the finest grid.

A multigrid must be matched with a multitemplate. The more grids there are in the multigrid, the larger the size of the template will be, and the more patterns will be extracted; however, since the effective size of the template does not change, the time and memory required will not increase exponentially. Liu [29] pointed out that reconstruction performance will not be advanced substantially, when the number of multigrids is more than three layers; hence most researchers have used multigrids with three grids. In a multigrid system, simulation is first performed on the coarsest grid. Once the coarse simulation is completed, the simulated values are assigned to the correct grid locations on a finer grid to be used as conditioning data on the finer grid. The distance between adjacent grids of a multigrid is expended based on the formula

$$[(T_x - 1)2^{M-i} + 1][(T_y - 1)2^{M-i} + 1]. \tag{7}$$

The size of the unexpended template is $T_x \times T_y$, matching the finest grid. M is the multigrid grid number. i ($i = 1, 2 \ldots, M$) is the grid order number. Figure 1 shows a three-grid.

III. THREE-STEP SAMPLING

A. Variability and continuity between adjacent layers

The key issue in the layer-by-layer method is how to control continuity and variability between adjacent layers during the reconstruction procedure [30]. Continuity is the consistency and similarity of patterns in the corresponding position between adjacent layers, and variability is the difference and variety of the patterns in the corresponding position between adjacent layers. It is because of the continuity and variability that the statistical characteristics and configuration of the direction perpendicular to the layers have an opportunity to match the TI. It is more important and difficult to control variability between adjacent layers than continuity.

Continuity and variability between adjacent layers are confirmed directly by the matched patterns, and the matched patterns are confirmed by the pattern set, matching rules, and condition data (sampling points). However, for specific TIs and SNESIM, the pattern set and matching rules are also specific; hence how to select the sampling points is very important. By controlling the sampling points, continuity and variability among adjacent layers can be controlled directly, and the local porosity, pore configuration, connectivity, and other statistical characteristics be controlled indirectly.

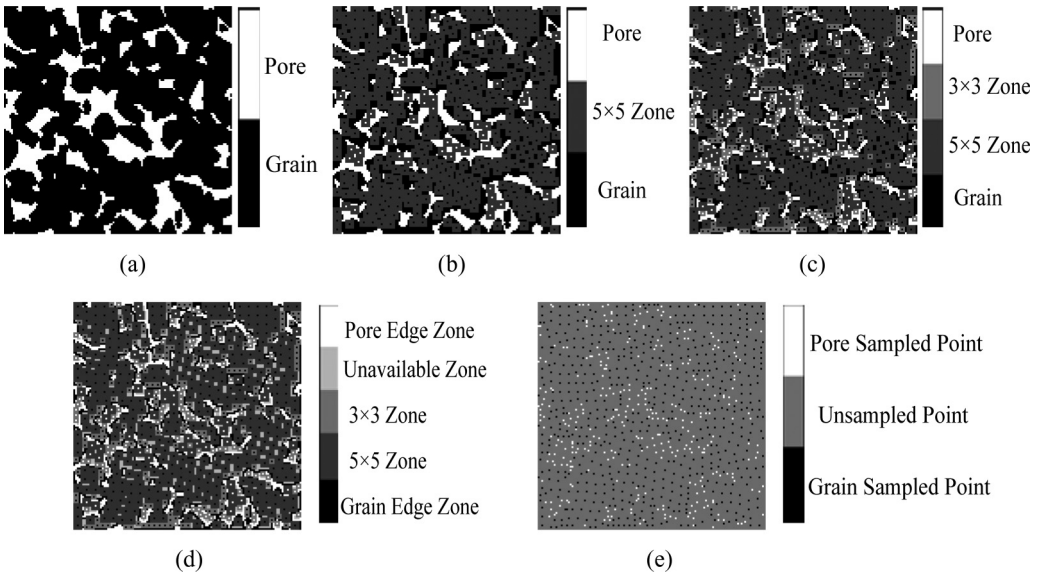

FIG. 2. The procedure of three-step sampling. (a) The TI with size of 128 × 128 pixels. (b) The result after sampling using the 5 × 5 template. (c) The result after sampling with the 3 × 3 template. (d) The invalid sampling area and the edge area after the first two sampling steps. (e) The final selected sampling points.

A specific sampling procedure includes selecting the sampling rate and sampling points' locations. It is obvious that a high sampling rate leads to strong constraints and continuity between adjacent layers; conversely, a lower sampling rate leads to weaker constraints and strong variability between adjacent layers. Consequently, the sampling rate is a specific value between zero and 1, and there is no uniformity restriction; hence, different algorithms have different descriptions and requirements.

In this paper, the center of an N×N zone belonging to one phase is used as the sampling point. Obviously, the size of the zone affects the sampling rate directly and the performance of the reconstruction indirectly. If the size is too small and the sampling rate too high, then the reconstruction will have less variability and stronger continuity; conversely, if the size is too large and the sampling rate too low, the reconstruction will have excessively strong variability and lower continuity. Consequently, there are three key issues:

First, how large a sampling template size can create balance between the continuity and variability of adjacent layers?

Second, if the minimum size of an N×N sampling template is selected as 3 × 3, then obviously substantial edge area cannot be sampled, if the size is less than 3 × 3, but such edge areas should be sampled, because they embody the details of the pore (grain). Then, how do we choose the sampling points that form an edge area?

Third, based on the layer-to-layer method, the statistics of a TI can be carried to the layer in the horizontal direction based on MPS, but that does not ensure that the statistical characteristics of the vertical direction (Z direction) will also match the TI. Hence, what measures can be used to ensure that the reconstruction's statistical characteristics in the vertical direction (Z direction) match the TI?

This paper proposes three-step sampling to overcome these three problems.

B. The principle of three-step sampling

The principle of three-step sampling is illustrated in Fig. 2. Figure 2(a) shows the TI. The important components of three-step sampling include the following steps. In the first step, the image is scanned using a 5 × 5 sampling template; the central node of the template, which is entirely pore (grain), is marked as a sampling point, the number of sampling points is recorded, and this sampled area is labeled, as shown in Fig. 2(b). In the second step, the remaining portion of the image other than the labeled area is scanned using a 3 × 3 sampling template, and the process stated in the first step is performed again, as shown as Fig. 2(c). In the third step, the unavailable sampling area is labeled, and the number of pixels is recorded. The unavailable sampling area is the area that was not included in the first two steps, but the pixels of the area belong to one phase, when scanning this area using the 3 × 3 template, as shown in Fig. 2(d). In the fourth step, the remaining area, the edge area, is marked, and the number of pixels is recorded, as shown in Fig. 2(d). In the fifth step, the third set of sampling points is selected, according to the algorithm described in the following section. Finally, all of the selected sampling points are shown in Fig. 2(e).

The reconstructed results using different sized sampling templates are compared in Fig. 3. The original image is shown in Fig. 2(a). The reconstructed results using the 3 × 3 sampling template show excessively strong continuity; in particular, the larger pores could not move even after ten layers, as in the area circled with yellow in Figs. 3(a) and 3(b). The reconstruction using the 5 × 5 sampling template shows excessively strong variability; even the bigger pores vary too widely at the first reconstructed layer, as in the area circled with yellow in Fig. 3(c), and the porosity drops too sharply, since many little pores could not be sampled by the sampling template, as indicated for the No. 11 layer shown in Fig. 3(d). In addition, the statistical characteristics of the reconstruction using the

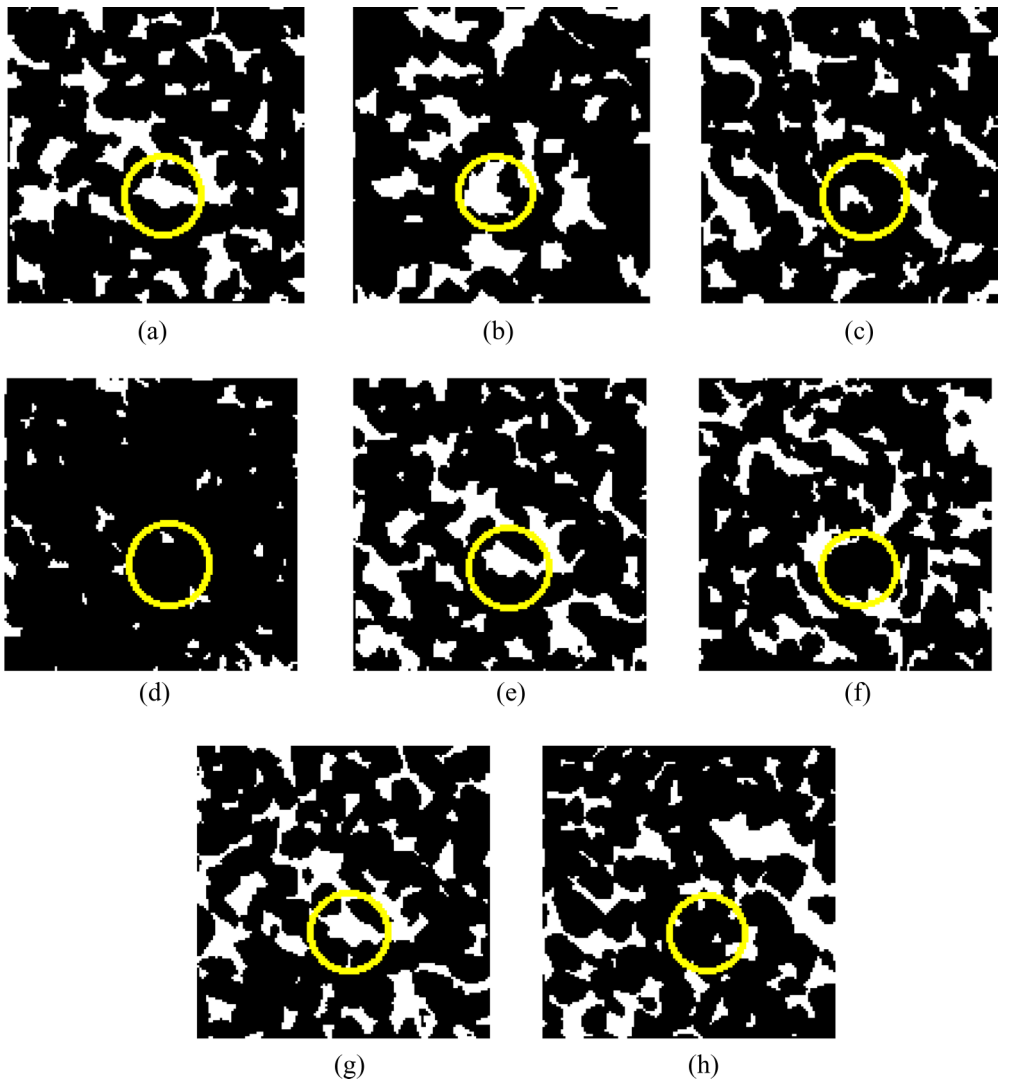

FIG. 3. (Color online) Comparison between reconstructed results using different size sampling templates. The TI is shown in Fig. 2(a); (a) and (b) are, respectively, the No. 1 and No. 11 layers using only the 3×3 sampling template; (c) and (d) are, respectively, the No. 1 and No. 11 layers using only the 5×5 sampling template; (e) and (f) are, respectively, the No. 1 and No. 11 layers using the 5×5 and 3×3 sampling templates combined; and (g) and (h) are, respectively, the No. 1 and No. 11 layers of the CT.

5×5 or 3×3 sampling template, respectively, could not match the TI, even though the measure that will be proposed in the next section was used. The reconstruction using the 5×5 and 3×3 sampling templates together shows better balance between variability and continuity, such as in the area circled with yellow color in Figs. 3(e) and 3(f); it is similar to the computed tomography (CT) sample shown in Figs. 3(g) and 3(h).

Considering the appropriate number and location of sampling points in the first two-step sampling process, the first issue proposed at the former part was solved properly. The last two issues will be solved in the next step, which is edge area sampling. This procedure is the key segment of the entire algorithm.

C. The edge sampling procedure

Edge sampling involves selecting a number of sampling points satisfying specific condition data from the edge area. While reconstructing other layers, the number N_e of edge sampling points for pore and grain can be expressed as

$$N_e^{i,j} = N - N_5^{i,j} - N_3^{i,j} \pm N_{p1}^{i,j} \pm N_{p2}^{i,j}, \quad (i = 2,3,\ldots,L_{\max}; j = 1,2), \tag{8}$$

where i denotes the reconstructing layer number, and $j = 1$ and $j = 2$ denote the pore and grain, respectively. The sign "+" is selected when $j = 1$, comparing "–" when $j = 2$. To control the porosity, all sampling points N must be confirmed to be equal to the first layer's numbers. N_5 and N_3 are the sampling points numbers sampled using the 5×5 and 3×3 templates, respectively and N_{p2} are the adjustment points numbers, for the first parameter indicating the difference between the porosities of a former layer and the TI, and for the second parameter indicating the difference between the porosities of the entire reconstructed part and the TI. It is obvious that the theoretical scope of the sampling rate is

TABLE I. The edge sampling procedure.

1.	Calculate the X direction (or Y direction) ACF of TI, and get the controlling points set TI(r)
2.	Process the discontinuous and isolated points of the reconstructed part
3.	for $[r = \min(L_i, A_e);\ r \geqslant A_b;\ r = r - d]$
4.	Calculate ACF rec(r) of the reconstructed part $(0 \leqslant x < W;\ 0 \leqslant y < H;\ 0 \leqslant z < L_i)$
5.	for $(0 \leqslant x < W;\ 0 \leqslant y < H)$
6.	if $(\text{rec}(r) > TI(r);\ c[z-r][y][x] = p;\ e[y][x] = p)$
7.	Delete $(e[y][x] = p)$;
8.	++count
9.	else if $(\text{rec}(r) < TI(r);\ c[z-r][y][x] = g;\ e[y][x] = p)$
10.	Delete $(e[y][x] = p)$;
11.	++count;
12.	if $(N_E^{i,1} - \text{count} < N_e^{i,1})$
13.	Break;
14.	End 3;
15.	Count the number with $e[y][x] = p$, and signed by s_p, $0 \leqslant x < W;\ 0 \leqslant y < H$;
16.	if $(s_p > N_e^{i,1})$
17.	Select sampling point $N_e^{i,1}$ with pore phase from s_p randomly;
18.	Else
19.	Set the point with $e[y][x] = p$ as sampling points, then select $N_e^{i,1} - s_p$ pore phase sampling points from the deleted points randomly;
20.	Select $N_e^{i,2}$ sampling points with grain phase as the steps 3–19.

less than 11%–4%, and it relates to the complexity of the TI structure.

After confirming the number of sampling points, the next issue is selecting the sampling points N_e from the edge area for the sampling process to ensure that the variability between adjacent layers of the reconstructed result matches the statistical characteristics of the TI. The autocorrelation function (ACF) was used by the simulated annealing algorithm because it indicates the statistical characteristics of spatial correlation of different phases [31–34]; hence, it is also used in this paper as the constraint conditions for selecting the edge sampling points. The definition of ACF will be provided in Sec. III B 2.

The ACF of the X direction (or Y direction) of the TI can be used as a controlling condition for the vertical direction (Z direction) of 3D reconstruction. Considering the continuity and the general trend of ACF, with high correlation (value) for closer points, the limited edge sampling points, the points with large ACF values, are selected as controlling condition points. A_b is the first controlling point (the minimum r within the selected set), A_e is the last controlling point (the maximum r within the selected set), and d is the distance between adjacent controlling points. The edge sampling procedure is shown in Table I.

The array $c[z][y][x](0 \leqslant x < W;\ 0 \leqslant y < H;\ 0 \leqslant z < L_{\max})$ indicates the reconstructing 3D cube, the array $e[y][x]$ indicates the edge sampling area, the sign $N_E^{i,1}$ indicates the whole number of pore edge points, and L_i is the number of layers to be reconstructed currently.

Remember that although the ACF is selected as the constraining condition in this paper, it is only the constraining condition for selecting the sampling points in the edge sampling step, but the reconstructed patterns are produced using MPS; hence, it is completely different from the algorithm based on two-point statistics. This constraining condition is weak, but it can control the continuity and variability of adjacent layers effectively. Now, the all questions proposed in the former section can be resolved perfectly.

IV. RESULTS AND DISCUSSION

A. Background and results

Some researchers, such as Hajizadeh *et al.* [26] and Tahmasebi *et al.* [14,15], have proposed an original kind of reconstructing sequence. Before reconstructing the layers, four frames for the front, right, back, and left sides of the 3D volume are reconstructed. First, the front face of the 3D volume, conditioned to overlap the boundary with the TI, is constructed. Then, the right face of the 3D volume, conditioned to boundaries overlapping with the front face and the TI, is constructed, and so on, until all four faces are constructed. Figure 4 illustrates the procedure schematically. Once the porous medium's frame is constructed, the reconstruction will be begun at the bottom. During reconstruction, the boundaries formed by the reconstructing layer and the four exterior faces will be treated as hard data.

Porous media of Berea sandstone samples were selected for reconstruction. The 2D image used as the TI is shown in Fig. 2(a), which was generated using micro-CT scanning with a resolution of 10 μm and a size of 128 × 128 pixels. The sample exhibits little variability, the TI having a porosity of 0.213, close to the porosity of 0.206 for the 3D sample. The template size used in the reconstruction was 9 × 9, the number of multigrids was 3, and the minimum number of SNESIM replicates was 10.

The reconstructed Berea sandstone result is shown in Figs. 5(a)–5(c); it is compared with the 3D image of the original sample in Figs. 5(d)–5(f). The side views of the reconstructed result are compared with the original sample. They indicate that the reconstructed result has reproduced the

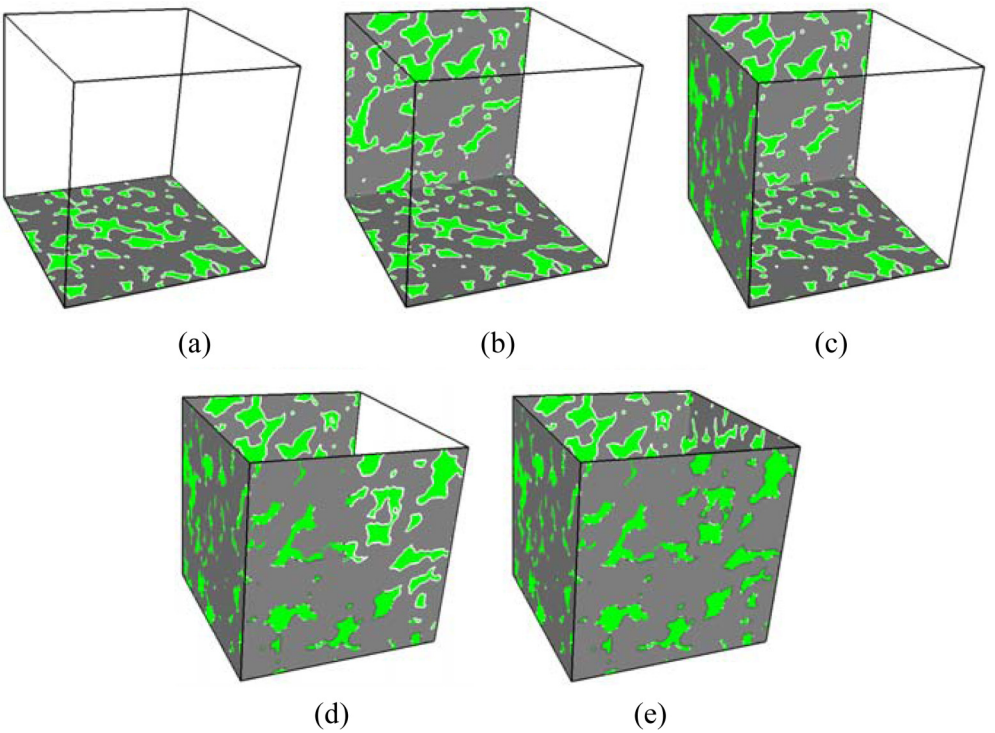

FIG. 4. (Color online) Five initial steps for constructing the external view of the Berea sandstone.

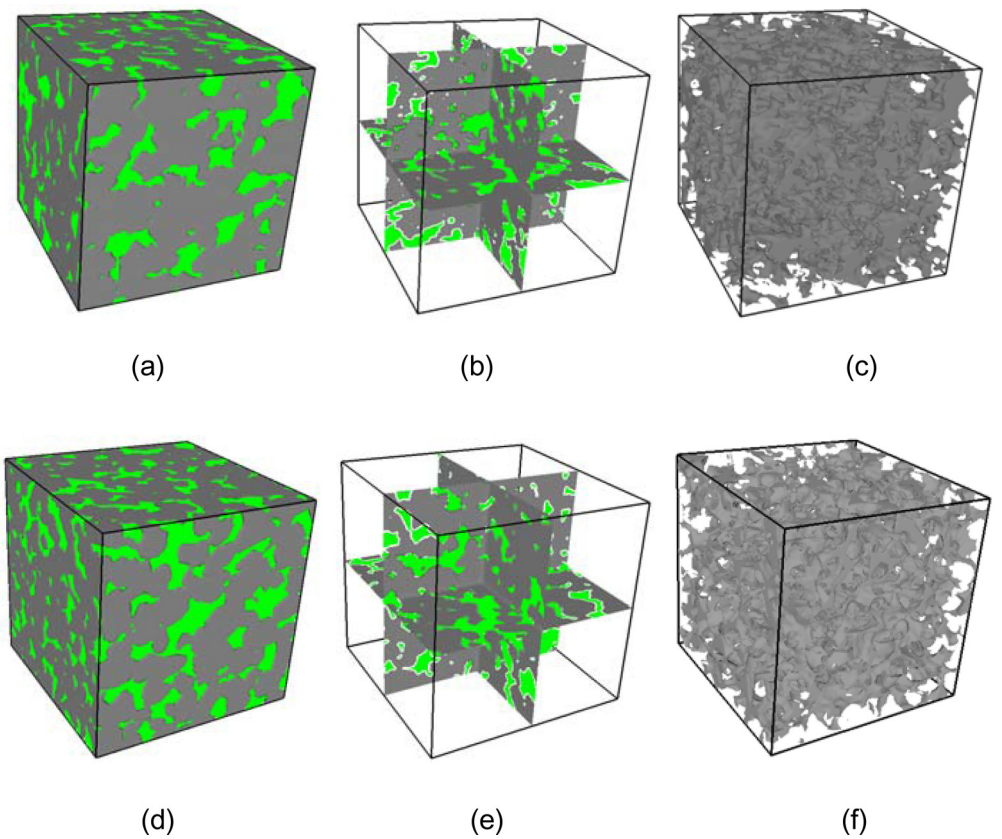

FIG. 5. (Color online) Visual comparison of spatial pore connectivity of the micro-CT image of Berea sandstone with that of a corresponding 3D reconstruction. (a) 3D exterior view of the reconstructed result, (b) a cross section of the reconstructed result, and (c) the perspective image of the reconstructed result. (d) Micro-CT sample, (e) a cross section of micro-CT sample, and (f) the perspective image of the micro-CT sample.

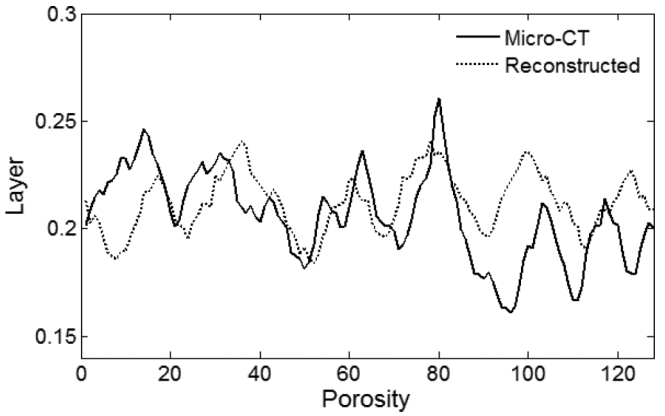

FIG. 6. Comparison of the porosity distribution in the reconstructed Berea sandstone with that of its micro-CT sample.

structure and connectivity of the original sample. Thus, at the visual level, the three-step sampling method is capable of preserving the connectivity of the sample in the direction of stacking the 2D images that it reconstructs, as well as the variability in the spatial distribution of the pores.

B. Porosity distribution

The average porosity of the reconstructed result is 0.213, little more than the 0.206 porosity of the Berea sandstone sample micro-CT, but same as the 0.213 of the TI; hence, the overall porosity was preserved well. The porosity variations of each layer in the micro-CT sample are compared with the reconstructed result shown as Fig. 6. Comparison with the corresponding curves confirms that the fluctuating patterns of local porosity in the vertical direction are very similar.

C. Two-point correlation function (ACF)

The void-void (pore-pore) ACF is defined by

$$R(u) = \frac{\langle [I(r) - \phi][I(r+u) - \phi] \rangle}{\phi - \phi^2}, \tag{9}$$

where the averaging is over all locations r within the volume, and $I(r)$ is an indicator function such that $I(r) = 1$, if r is in the pore space, and $I(r) = 0$ otherwise. The porosity is simply $\phi = \langle I(r) \rangle$.

We compare the ACFs of the TI, the micro-CT image of the Berea sandstone, and the reconstructed porous result. The ACFs were computed in the three orthogonal directions for which we had access to the full 3D image. The comparisons for the micro-CT medium of the Berea sandstone and reconstructed result are presented in Fig. 7. It is clear that the ACFs of the reconstructed result match the actual data very well.

D. Lineal path function (LPF)

The LPF, also called multiple-points connectivity probability, is a measure of the connectivity of the system within an image. It is a concept more general than the coordination number that characterizes the local connectivity of the pores and is concerned with determining the probability of having a sequence or a continuous string of r points in a structure in any given direction, such as pores in a pore space. It is defined by

$$L(\vec{u},\vec{u}+\vec{r}) = \text{Prob}(\vec{u},\vec{u}+\vec{r}) = \begin{cases} 1 & \vec{r} \in V_0 \\ 0, & \text{else} \end{cases}, \tag{10}$$

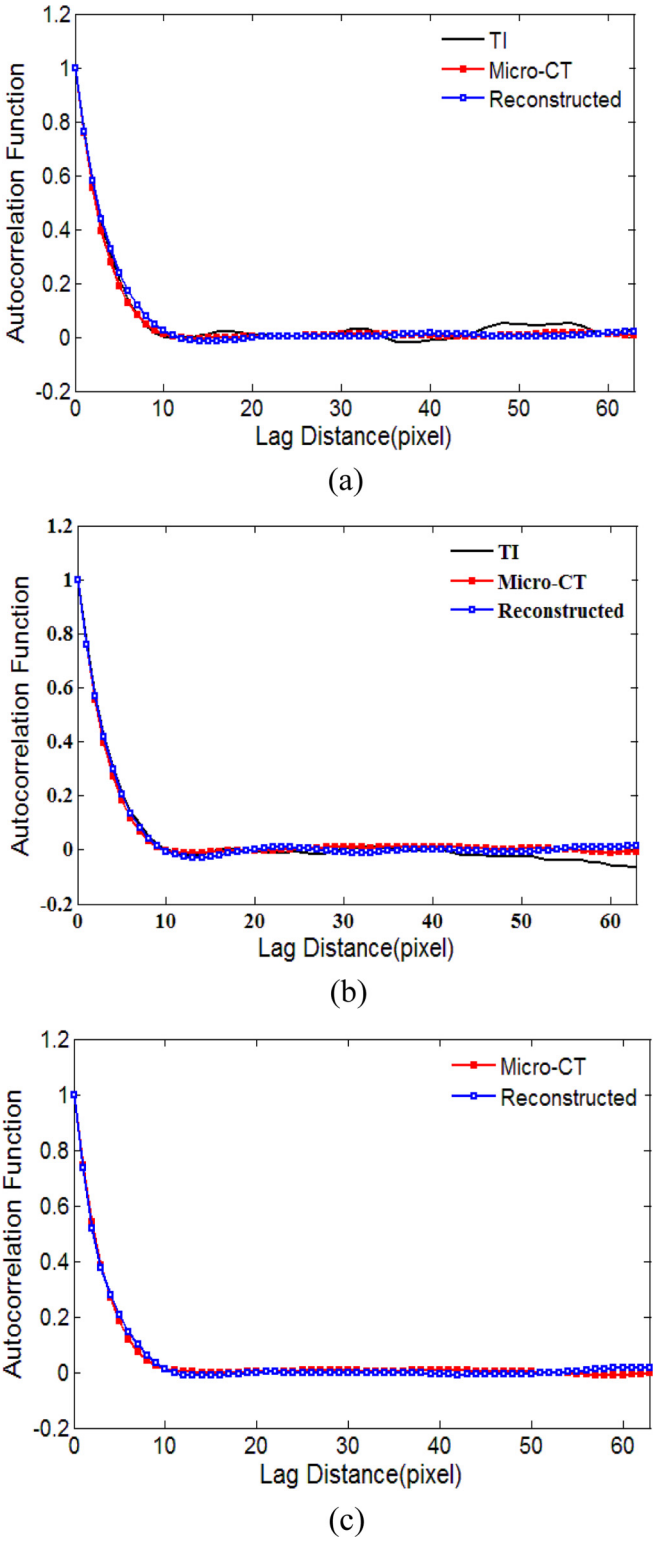

FIG. 7. (Color online) Comparison of ACFs for three images, in (a) the x direction, (b) the y direction, and (c) the z direction (perpendicular to the page and reference with the y direction of TI).

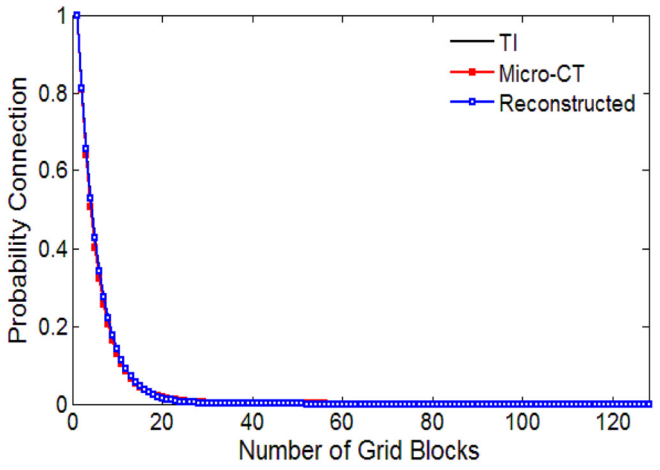

(a)

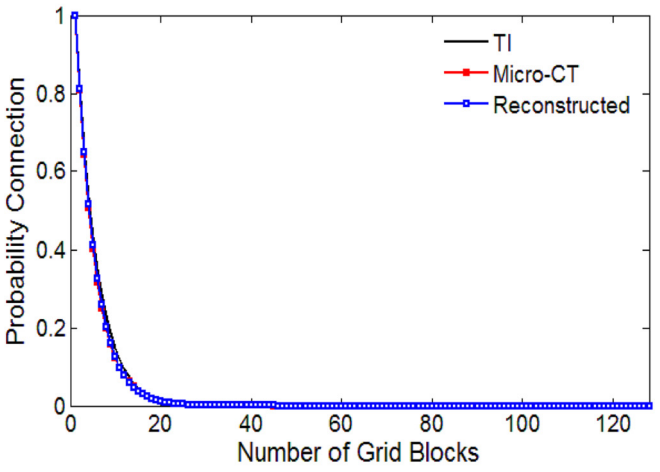

(b)

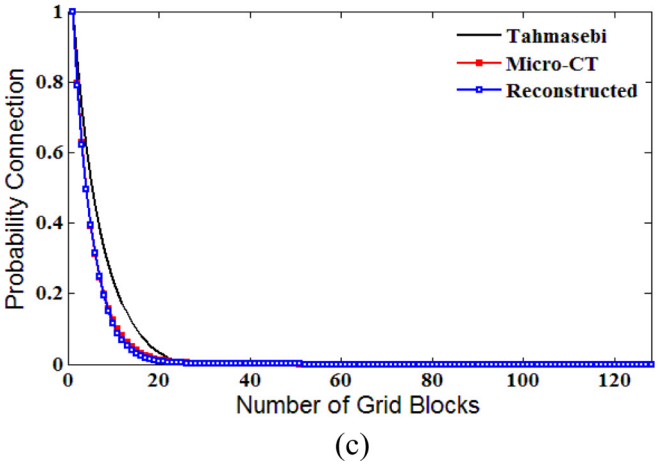

(c)

FIG. 8. (Color online) Comparison of the LPFs for TI, micro-CT image, and reconstructed result of the Berea sandstone in the (a) x, (b) y, and (c) z directions.

where $\vec{r}$ is the length of a line in the specific direction. The advantage of such a connectivity function, in addition to its global nature, is that it allows one to account for the curvilinearity of the system by considering a tolerance core around a target direction.

The results for the Berea sandstone in the three orthogonal directions are shown in Fig. 8. The sets of results indicate the accuracy of the reconstructed result, but the result which was reconstructed by the method of Tahmasebi [14] has more continuity than TI, as indicated on Fig. 8(c).

E. Flow characteristics

Although the comparisons discussed thus far indicate the accuracy of the proposed algorithm, they were based on limited statistics. It is entirely possible for two models to have similar such statistics, but very different flow characteristics. As a more critical test of the quality of the reconstructed media, we can consider the estimation of the relative permeabilities for two-phase flow. This is a difficult test, because relative permeability is critically dependent on the distribution of pore sizes and the 3D spatial connectivity of a porous medium, as well as capillary pressure effects and the wetting characteristics of the rock. A common way to model two-phase flow in a complex 3D porous medium is to replace the pore structure with an equivalent network of pores and connecting throats. It has been shown that pore-throat networks derived directly from a real porous medium can properly capture the relevant statistical and topological properties associated with that medium. In this work, we used the method proposed by Dong and Blunt [35], who used the maximal ball algorithm to extract the sizes of the pores and throats from images of a porous medium. This algorithm was developed to extract topologically disordered networks of pores and throats with parametrized geometry and interconnectivity. Figure 9 shows the pore network model structure of the reconstructed result compared with the actual 3D image. Table II compares some important parameters of the pore and throat in the pore network model from the Berea sandstone and its 3D reconstructed medium. The two sets of results agree well, almost all parameters of the reconstructed porous media being in accordance with the micro-CT of the porous media.

After the pore network equivalent model was constructed, two-phase flow simulations of oil and water in the Berea sandstone were conducted. We simulated the primary drainage—displacements of a wetting phase (water) by a nonwetting phase (oil)—followed by the reverse imbibition process. The simulator combines the topologically disordered network that represents the image and its reconstructed version with detailed two-phase flow displacement mechanisms for any sequence

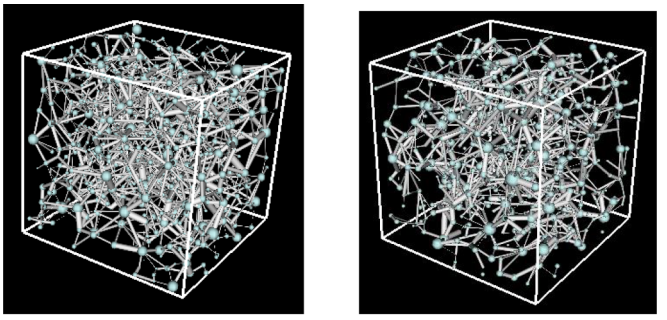

(a) (b)

FIG. 9. (Color online) Pore network model: (a) micro-CT sample and (b) reconstructed result.

TABLE II. Some important parameters of the pore and throat in the pore network.

	Micro-CT porous media	Reconstructed porous media
Average shape factor	0.0298	0.0298
Average size of pore radius (m)	$1.75 \times 10^{--5}$	1.77×10^{-5}
Average size of throat radius (m)	7.80×10^{-6}	8.31×10^{-6}
Average volume of pore (m^3)	4.33×10^{-13}	4.80×10^{-13}
Average volume of throat (m^3)	3.26×10^{-14}	4.35×10^{-14}
Average radius size ratio of pore and throat	0.289	0.274
Average coordination number	4.57	3.89
Effective permeabilities (mD)	1189	1175

of water and oil flooding and any wettability of the pores' surface. During the primary flooding, the pore network is assumed to be strongly wetted by the wetting phase (water for the water-oil systems and oil for the oil-gas system, or oil in the Berea sandstone), with a receding contact angle of 0° and an advancing contact angle of 0°.

During the secondary flooding, the receding contact angle was set as 50° and the advancing contact angle was set as 60°. The network size was $128 \times 128 \times 128$, the oil and water density were assumed to be 900 and 1000 kg/m^3, respectively, and the water-oil surface tension was taken to be 3×10^2 N/m, with the oil and water viscosities assumed to be 1.05×10^3 and 1.0×10^3 kg/ms, respectively. The computed results for both the reconstructed result and the original 3D Berea sandstone are presented in Fig. 10. The agreement between the two sets of results is excellent, indicating the accuracy of the reconstructed model. This provides strong evidence that the proposed stochastic 3D pore space reconstruction algorithm can reproduce the spatial statistics and the microstructure of a porous medium from a single 2D image.

V. CONCLUSION

We proposed and developed a three-step sampling method with the goal of reconstructing 3D porous media from a single 2D image, using an MPS method to preserve the long-range (global) connectivity of the pore space. Based on one layer of a 2D TI, a second layer was reconstructed, which was then used to reconstruct a third layer, and so on. The reconstructed layers were then stacked together to generate the entire reconstructed 3D porous medium. To perform this successfully, the key point is to ensure the continuity and variability between the adjacent layers that are consistent with the statistical characteristics of the TI. By selecting the number and location of sampling point appropriately, not only the continuity and variability, but also other statistical characteristics can be controlled. We proposed and developed a sampling method consisting of three steps: The center of the 5×5 and 3×3 zone that belong to one phase were selected as two sampling points successively at the first two steps, and the third part of the sampling points was selected from the remaining zone (edge area) under the constraint of a two-point correlation function at the third step. The continuity and variability between the adjacent layers were considered and were ensured matching TI at the whole sampling process. We tested our method on Berea sandstone. The properties of the reconstructed result agreed well with the actual samples. Considering its accuracy, we believe that the algorithm we suggested in this paper has potential applications to reconstruction of a wide variety of anisotropic systems, some of which will be studied and reported on in the near future.

ACKNOWLEDGMENTS

This work was supported by the National Natural Science Foundations of China (Grants No. 60972130 and No. 61372174), and the Fundamental Research Funds for the Central Universities (Grant No. ZYZ2012056).

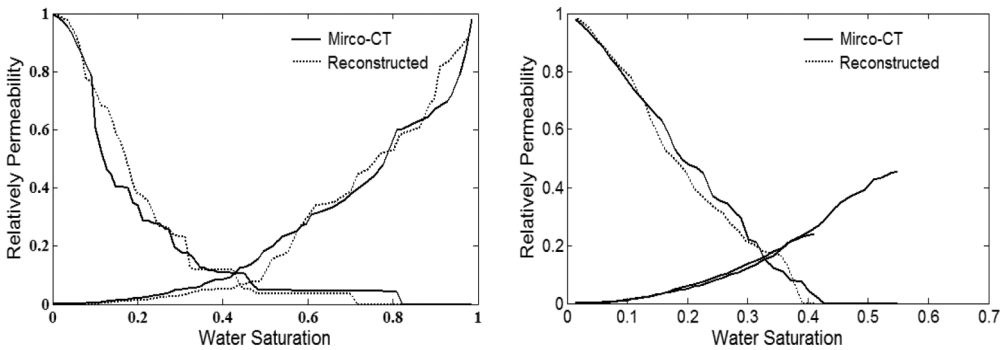

FIG. 10. Drainage and imbibition relative permeability curves of the 3D micro-CT image and the 3D reconstructed result. (a) Drainage and (b) imbibition.

[1] P. Goovaerts, *Geostatistics for Natural Resources Evaluation* (Oxford University Press, New York, 1997).
[2] C. V. Deutsch and A. G. Journel, *GSLIB: Geostatistical Software Library and User's Guide*, 2nd ed. (Oxford University Press, New York, 1998).
[3] F. D. E. Latief, B. Biswal, U. Fauzi, and R. Hilfer, Physica A (Amsterdam, Neth.) **389**, 1607 (2010).
[4] B. Biswal, P.-E. Oren, R. J. Held, S. Bakke, and R. Hilfer, Phys. Rev. E **75**, 061303 (2007).
[5] F. Sajjad, J. Saeid, and M. Mohsen, Physica A (Amsterdam, Neth.) **392**, 4772 (2013).
[6] F. B. Guardiano and R. M. Srivastava, in *Geostatistics Tróia '92*, edited by A. Soares (Kluwer Academic, Amsterdam, 1993), Vol. 1, pp. 133–144.
[7] S. Strebelle and C. Claude, Math. Geosci. **46**, 171 (2013).
[8] S. Strebelle, Math. Geol. **34**, 1 (2002).
[9] S. Strebelle, Ph.D. thesis, Stanford University, 2000.
[10] B. Arpat, Ph.D. thesis, Stanford University, 2005.
[11] B. Arpat and J. Caers, Math. Geol. **39**, 177 (2007).
[12] T. Zhang, P. Switzer, and A. G. Journel, Math. Geol. **38**, 63 (2006).
[13] P. Tahmasebi and M. Sahimi, Phys. Rev. Lett. **110**, 078002 (2013).
[14] P. Tahmasebi and M. Sahimi, Phys. Rev. E **85**, 066709 (2012).
[15] P. Tahmasebi, A. Hezarkhani, and M. Sahimi, Comput. Geosci. **16**, 779 (2012).
[16] J. Straubhaar, P. Renard, G. Mariethoz, R. Froidevaux, and O. Besson, Math. Geosci. **43**, 305 (2011).
[17] G. Mariethoz, P. Renard, and J. Straubhaar, Math. Geosci. **43**, 783 (2011).
[18] J. Straubhaar, A. Walgenwitz, and P. Renard, Math. Geosci. **45**, 131 (2013).
[19] Z. Xu, Q. Z. Teng, X. H. He, X. M. Yang, and Z. J. Li, J. Pet. Sci. Eng. **100**, 71 (2012).
[20] G. Mariethoz, P. Renard, and J. Straubhaar, Water Resour. Res. **46**, W11536 (2010).
[21] E. Meerschman, G. Pirot, G. Mariethoz, J. Straubhaar, M. V. Meirvenne, and P. Renard, Comput. Geosci. **52**, 307 (2013).
[22] T. Tran, Comput. Geosci. **20**, 1161 (1994).
[23] H. Okabe and M. J. Blunt, Phys. Rev. E **70**, 066135 (2004).
[24] H. Okabe and M. J. Blunt, J. Pet. Sci. Eng. **46**, 121 (2005).
[25] K. Mahmud, G. Mariethoz, J. Caers, P. Tahmasebi, and A. Baker, Water Resour. Res. **50**, 3088 (2014).
[26] A. Hajizadeh, A. Safekordi, and F. A. Farhadpour, Adv. Water Resour. **34**, 1256 (2011).
[27] M. Huysmans and A. Dassarues, Math. Geosci. **43**, 521 (2011).
[28] J. B. Boisvert, M. J. Pyrcz, and C. V. Deutsch, Nat. Resour. Res. **16**, 313 (2007).
[29] Y. H Liu, Comput. Geosci. **32**, 1544 (2006).
[30] A. Hajizadeh and Z. Farhadpour, Transp. Porous Media **94**, 859 (2012).
[31] C. L. Y. Yeong and S. Torquato, Phys. Rev. E **57**, 495 (1998).
[32] C. L. Y. Yeong and S. Torquato, Phys. Rev. E **58**, 224 (1998).
[33] D. D. Chen, Q. Z. Teng, X. H. He, Z. Xu, and Z. J. Li, Phys. Rev. E **89**, 013305 (2013).
[34] D. D. Chen, X. H. He, Q. Z. Teng, Z. Xu, and Z. J. Li, Physica A (Amsterdam, Neth.) **415**, 240 (2014).
[35] H. Dong and M. J. Blunt, Phys. Rev. E **80**, 036307 (2009).